

Reinforcement Learning for Control of Valves

Rajesh Siraskar^{1,*}

Faculty of Engineering, Environment and Computing, Coventry University, UK

Abstract

This paper is a study of reinforcement learning (RL) as an optimal-control strategy for control of nonlinear valves. It is evaluated against the PID (proportional-integral-derivative) strategy, using a unified framework. RL is an autonomous learning mechanism that learns by interacting with its environment. It is gaining increasing attention in the world of control systems as a means of building optimal-controllers for challenging dynamic and nonlinear processes. Published RL research often uses open-source tools (Python and OpenAI Gym environments). We use MATLAB's recently launched (R2019a) Reinforcement Learning Toolbox™ to develop the valve controller; trained using the DDPG (Deep Deterministic Policy-Gradient) algorithm and Simulink® to simulate the nonlinear valve and create the experimental test-bench for evaluation. Simulink allows industrial engineers to quickly adapt and experiment with other systems of their choice. Results indicate that the RL controller is extremely good at tracking the signal with speed and produces a lower error with respect to the reference signal. The PID, however, is better at disturbance rejection and hence provides a longer life for the valves. Successful machine learning involves tuning many hyperparameters requiring significant investment of time and efforts. We introduce “Graded Learning” as a simplified, application oriented adaptation of the more formal and algorithmic “Curriculum for Reinforcement Learning”. It is shown via experiments that it helps converge the learning task of complex non-linear real world systems. Finally, experiential learnings gained from this research are corroborated against published research.

Keywords: Curriculum Learning, Graded Learning, MATLAB, Optimal-control, Reinforcement Learning, Valve control

1. Introduction

Reinforcement learning (RL) is a machine learning technique that mimics learning abilities of humans and animals. RL applications have been used by OpenAI to program robot-hands to manipulate physical objects with unprecedented human-like dexterity (openai.com, 2018), by Stanford's CARMA program for autonomous driving (Vitelli and Nayebi, 2016) and studied for faster de novo molecule design (Olivecrona et al., 2017).

This paper studies application of RL as an optimal-control strategy. RL promises better control by interacting directly with the plant and *learning* optimal-control without the need of accurate modeling of the plant.

Valves were selected as the controlled plant as they are ubiquitous in process control and employed in almost every conceivable manufacturing and production industry. Industrial process loops can involve thousands of valves and can be impossible to model accurately.

PID (proportional-integral-derivative) is the de facto control strategy covering more than 95% of industrial controllers (Desborough and Miller, 2002). However applying this conventional strategy, can potentially affect quality and efficiency of processes and increase substantial costs.

Connecting a computer to a real physical plant and have the RL agent learn through direct interaction may not always be feasible and a practical approach often adopted, involves simulating the real plant as close as possible and is the approach we use. MATLAB Simulink® is used to simulate a nonlinear valve, an industrial process, the agent training circuit and finally a unified RL-PID validation circuit. The controller, called an “agent” in RL terminology, is trained using MATLAB's recently launched (R2019a) Reinforcement Learning Toolbox™ using the DDPG (Deep Deterministic Policy-Gradient) algorithm.

Graded Learning, a technique discovered accidentally during this research is a simple procedural method to efficiently train a RL agent on complex tasks and in effect is the most simplified form of the more formal method known as “Curriculum Learning” (Narvekar et al., 2020).

Summary research contributions of this work:

1. Understanding RL as an optimal-control strategy.
2. A methodology to assist practising plant engineers apply RL for optimal-control in industries. Design and simulation using MATLAB and Simulink, instead of the more demanding Open Source Python.
3. **Graded Learning:** A “coaching” method suitable for practicing engineers. It is an application oriented adaptation of the more formal and algorithmic “Curriculum for Reinforcement Learning”.

*Corresponding author

Email address: siraskar@coventry.ac.uk;
rajeshsiraskar@gmail.com (Rajesh Siraskar)

¹Author currently works as a Lead Data Scientist at Birlasoft, India.

4. Literature research on three studies of RL control for valves.
5. Experimental comparison of PID and RL strategies in a unified framework.
6. Stability analysis of the RL controller in time and frequency domains.
7. Experiential learning corroborated with published research.

Finally, while the valve is the focus of the paper, the methods are adaptable to any industrial system.

2. Reinforcement Learning Primer

In this section we take a brief look at conventional optimal-control solving methods, followed by an overview of RL, its connection with optimal-control and finally the DDPG algorithm selected for implementation.

Sutton and Barto’s book (2018) is the most comprehensive introduction to reinforcement learning and the source for theoretical foundations below.

2.1. Optimal Control and RL

Feedback controllers are traditionally designed using two philosophies: adaptive-control and optimal-control. Adaptive controllers are online learners and learn to control unknown systems by measuring real-time data. However, they are not optimized since the design process does not involve minimizing any performance metrics of the plant (Lewis et al., 2012).

Conventional optimal-control design, on the other hand, is performed off-line by solving Hamilton–Jacobi–Bellman (HJB) equations. According to Lewis et al. (2012) solving HJB equations require complete knowledge of the dynamics of the plant and according to Tedrake (2009) this in turn requires an engineered *guess* as a start.

Richard Bellman’s extension of the 19th century theory laid by Hamilton and Jacobi and Ronald Howard’s work in 1960 for solving Markovian Decision Processes (MDPs) all formed the foundations of modern RL. Bellman linked the dynamic system’s state with a “value-function”. Dynamic programming, which uses the *Bellman equation* and is a “backward-in-time” method, along with *temporal-difference* (TD) methods enabled building of optimal adaptive-controllers for discrete-time systems (i.e. time progression defined as $t, t + 1, t + 2\dots$) (Sutton and Barto, 2018).

2.2. Optimal Control

The Hamilton-Jacobi-Bellman (HJB) (1) provides a sufficient condition for optimality (Tedrake, 2009).

$$0 = \min_u \left[g(x, u) + \frac{\partial J^*}{\partial x} f(x, u) + \frac{\partial J^*}{\partial t} \right] \quad (1)$$

Controller *policies* (i.e. behavior) are denoted by π and optimum policies by π_* . If a policy $\pi(x, t)$, and a related cost-function $J^\pi(x, t)$, are defined such that π minimizes the right-hand-side of the HJB (1) $\forall x \in \mathbb{R}$ and all $t \in [0, T]$ to zero then:

$$J^\pi(x, t) = J^*(x, t), \quad \pi(x, t) = \pi^*(x, t) \quad (2)$$

Equation (1) assumes that the cost-function is continuously differentiable in x and t and since this is not always the case it does not satisfy all optimal-control problems. In (Tedrake, 2009), Tedrake shows that solving HJB depends on an engineered *guess*, for example a First-order Regulator is designed with a guessed solution $\pi(x, t) = -\text{sgn}(x)$. A Linear Quadratic Regulator is designed similarly. For complex, dynamic mechanical systems such initial solutions are hard to guess unless severely approximated and therefore in situations like these RL shows the relative ease with which real world optimal-control can be *learned*.

2.3. The RL framework

The core elements of RL are shown in Fig.1 (?), superimposed with equivalent control-system elements.

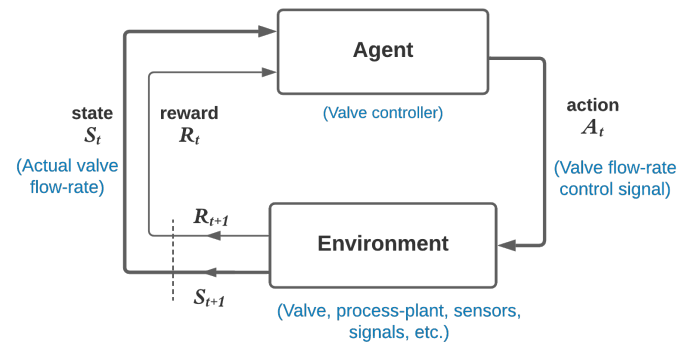


Figure 1: Building blocks of RL and equivalent control-system elements

The learner and decision-maker is called the *agent*. The agent interacts with its *environment* continually, selecting actions A_t , to which the environment responds by presenting a new situation S_{t+1} . The environment provides performance feedback via *rewards* (or penalties), R_{t+1} . Rewards are scalar values. Over time, the agent attempts to maximize (or minimize) the rewards and this *reinforces* good actions over bad enabling it to learn an optimal *policy*.

In control system terminology the agent is the controller being designed and the environment consists of the system outside the controller i.e. the valve, the industrial process, the reference signal, other sensors, etc. The policy is the optimal-control behavior the designer seeks. RL allows learning this behavior without having to be explicitly programmed or modeling the plant in excruciating detail.

Policy: The decision-making capability of the agent is based on a probability mapping of the best action to take vis-à-vis the state it is in. It is this mapping that forms the policy π_t , and $\pi_t(a|s)$ is the probability that the action $A_t = a$, if the state $S_t = s$.

Returns: Returns represent long-term rewards, gathered over time.

$$G_t = R_{(t+1)} + R_{(t+2)} + R_{(t+3)} \dots R_T \quad (3)$$

Discounting: Discounting provides a mechanism to control the impact of selecting an action that is immediate versus one

where rewards are received far into the future.

$$G_t = R_{(t+1)} + \gamma R_{(t+2)} + \gamma^2 R_{(t+3)} \cdots = \sum_{k=0}^{\infty} \gamma^k R_{((t+1)+k)}, \quad (4)$$

where γ , the *discount rate*, is a parameter $0 \leq \gamma \leq 1$.

Value-functions: As functions of state-action pairs these provide an estimate of how good it is to perform a given action in a given state. A reward signal provides feedback on how “good” the current action is, in an immediate short-term sense. In contrast, a value-function, provides a measure of “goodness” in the long-term and is defined in terms of future expected return.

The *value*, denoted $v_{\pi}(s)$, is the expected return for a state s , measured starting in that state s and following the policy π thereafter.

$$\begin{aligned} v_{\pi}(s) &= \mathbb{E}_{\pi}[G_t | S_t = s] \\ &= \mathbb{E}_{\pi} \left[\sum_{k=0}^{\infty} \gamma^k R_{(t+k+1)} \middle| S_t = s \right] \\ &= \sum_a \pi(a|s) \sum_{s',r} p(s', r|s, a) [r + \gamma v_{\pi}(s')] \end{aligned} \quad (5)$$

Equation (5) is referred to as the **Bellman equation** and forms the basis to approximately compute and learn v_{π} and is central to all RL algorithms.

Q-function: By including the action, $q_{\pi}(s, a)$ is defined as the expected return starting from state s , taking an action a and thereafter following policy π .

Q-learning: Q-learning is an off-policy TD control algorithm that allows iteratively learning the Q-value. For each state-action pair; the value $Q(s, a)$ is tracked. When an action a is performed in some state s , the two elements of feedback from the environment — the reward R and the next state S_{t+1} are used in the update shown in (6). α is the learning rate.

$$Q(S_t, A_t) \leftarrow Q(S_t, A_t) + \alpha [R_{t+1} + \gamma \max_a Q(S_{t+1}, a) - Q(S_t, A_t)], \quad (6)$$

where $V_t(s)$ is the estimate of $v_{\pi}(s)$ and $Q_t(s, a)$ the estimate of $q_{\pi}(s, a)$.

Optimal value-function: There always exists at least one optimal policy that guarantees the highest expected return denoted by v_* and an optimal action-value-function q_* .

Model-based and model-free RL methods: Accurate models of the environment allow “planning” the next action as well as the reward. An environment’s model means having access to a “table” of probabilities of being in a state, given an action; and associated rewards.

RL methods that use environment-models are called *model-based*, as opposed to simpler *model-free* methods. Model-free agents can only learn by trial-and-error (Sutton and Barto, 2018).

Actor-Critic methods: Actor-critic structure allows a forward-in-time class of RL algorithms that are implemented in real-time. The *actor* component, under a policy, applies an action to the environment and receives a feedback that is evaluated by the *critic*. Learning is a two-step mechanism — policy-evaluation performed by the critic, followed by policy-improvement, performed by the actor.

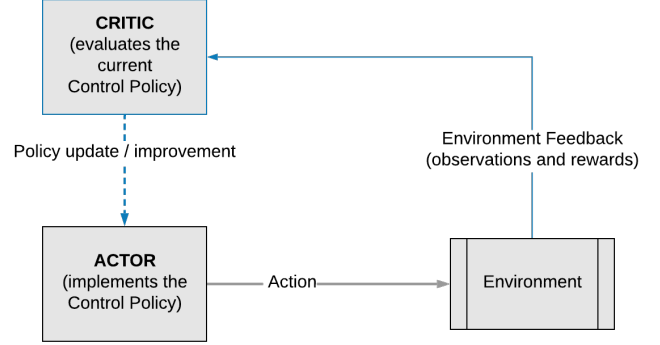


Figure 2: Actor-Critic architecture

2.4. The DDPG algorithm

MATLAB’s R2019a release provides six RL algorithms. DDPG was the only algorithm suitable for continuous action control (MathWorks, 2019a).

Lillicrap et al. (2015) introduced DDPG to overcome the shortcomings of the DQN (Deep Q-Network) algorithm which in turn was an extension of the fundamental Q-learning algorithm.

DDPG is a model-free, policy-gradient and off-policy (by use of a memory replay-buffer of previous *experiences*). As an actor-critic method, it uses two neural-networks. The actor network accepts the current state as the input and outputs a single real value (i.e the valve control signal) representing the action chosen from a continuous action space. The critic network performs the evaluation of the actor’s output (i.e. the action) by estimating the Q-value of the current state given this action. Actor network weights are updated by a *deterministic* policy-gradient algorithm while the critic weights are updated by gradients obtained from the TD error signal. The DDPG algorithm, therefore, simultaneously learns both a Q-function and a policy by interleaving them.

Exploration vs. exploitation: For RL, as is in humans, performance improvement is achieved by exploiting the best of past actions. However, to discover these, the agent must first explore untried actions. Balancing this discovery while continuously improving the best action is a common challenge. Various exploration-exploitation strategies have been developed.

DDPG uses the Ornstein-Uhlenbeck process (OUP) to enable exploration. Interestingly, OUP was developed for modeling Brownian particle velocities, with friction, and results in values that are *temporally correlated* (Uhlenbeck and Ornstein, 1930). The simpler additive Gaussian noise model causes abrupt uncorrelated changes from one time-step to another. OUP more

closely mimics real life actuators that exhibit inertia (Lillicrap et al., 2015).

The exploration policy π' is constructed by adding noise to the selected action, sampled from the OUP noise process \mathcal{N} .

$$\pi'(s_t) = \pi(s_t|\theta^\pi) + \mathcal{N}_t \quad (7)$$

3. Control Valves and RL

Control-valves modify the fluid flow rate, using an actuator mechanism, governed by a control system. Processing plants consist of large networks of control-valves designed to keep a process-variable under control to ensure quality of the end-product (IEEE-GlobalSpec, 1998).

3.1. Nonlinearity in valves

Control-valves, like most other physical systems, possess nonlinear flow characteristics such as friction and backlash. Friction in-turn has two components — *stiction*, the static friction, is the inertial force that must be overcome before there is any relative motion between the two surfaces and is the prime cause of dead-band in valves; while dynamic friction is the friction in motion (Choudhury et al., 2004a), (Choudhury et al., 2004b).

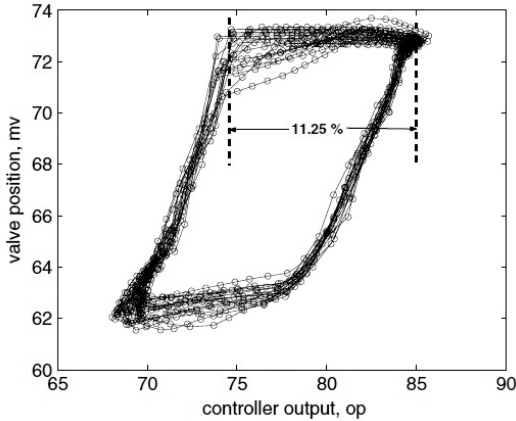


Figure 3: Actual valve movement trajectory (Choudhury et al., 2004a)

Nonlinearity can cause oscillatory valve outputs that in turn cause oscillations of the process output resulting in defective end-products, inefficient energy consumption and excessive wear of manufacturing systems (Choudhury et al., 2004a), (Shoukat Choudhury et al., 2005). According to Choudhury et al. (2004a), 30% of process-loop oscillation issues are due to control-valves, while Desborough and Miller (2002) reports that valves are the primary cause of 32% of surveyed inefficient controllers. Stiction in control-valves has been reported as the prime source of sustained oscillations in industrial control-loops (di Capaci and Scali, 2018).

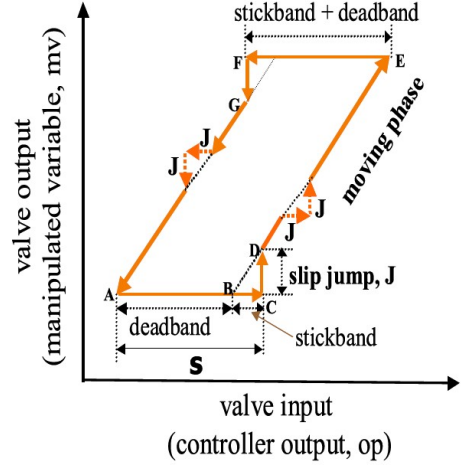


Figure 4: Nonlinear valve operating characteristics, with stiction (Choudhury et al., 2004a)

3.2. A mathematical valve model

RL requires experiences for training. Simulated environments often provide a quick and low-cost environment for training an agent. Since the objective of building a controller is for it to be used in the real-world, one must strive to create as accurate an environment as possible. This appears to contradict the claim made earlier that RL does not require an accurate system model — however it is assumed here that real physical environment is inaccessible, which on the other hand if accessible or available, could well allow the RL agent (controller) to learn directly from real experiences.

In this paper we use first-principles to model the valve as outlined in (di Capaci and Scali, 2018).

He and Wang (2010) describe the nonlinear memory dynamics of valve by $x_k = N_v(x_{k-1}, u_k)$, at a time-step k , where N_v is expressed by relation (8). While the controller outputs u , the actual position the valve attains is represented by x , where e_k represents the valve position error. f_s and f_D are the static (stiction) and dynamic friction parameters, dependent on the valve type, size and application. The “Experimental Setup” section describes the Simulink modeling of the valve.

$$x_k = \begin{cases} x_{k-1} + [e_k - \text{sign}(e_k)f_D], & \text{if } |e_k| > f_s \\ x_{k-1}, & \text{if } |e_k| \leq f_s \end{cases} \quad (8)$$

where $e_k = u_k - x_{k-1}$

3.3. RL for valve control: A literature research

The field of RL is relatively new and not many studies of its application for control of valves were found². A study of three publications is presented below with emphasis on overlapping areas of research.

²As of August, 2020, only 18 results showed up for “reinforcement learning AND valves AND control” on Scopus.

3.3.1. Throttle valve control

Control of a throttle valve is challenging due to the highly dynamic behavior of the spring-damper system and complex nonlinearities (Bischoff et al., 2013; Schoknecht and Riedmiller, 1999) as well as the multiple-input-multiple-output optimization required (Howell and Best, 2000).

Bischoff et al. (2013) use PILCO (probabilistic inference for learning), a data-efficient *model-based* policy search method. PILCO reduces model bias, a key problem of model-based RL, by learning the probabilistic dynamics of the model and then explicitly incorporating model uncertainty into long-term planning. PILCO is able to learn with only a few trials as against several thousand normally required for trial-and-error based model-free methods (Deisenroth and Rasmussen, 2011).

Valve dynamics are modeled using the flap angle, angular velocity and the actuator input. They must be controlled at an extremely high rate of 200 Hz without any overshoot (to avoid engine torque jerks). The controller learns by minimizing the expected sum of cost c over time.

$$\min_{\pi} J(\pi), J(\pi) = \sum_{t=0}^T \mathbb{E}_{s_t} c(s_t) \quad (9)$$

Fig.5 depicts a novel *asymmetric saturating* cost-function applied to achieve the zero-overshoot constraint. A trajectory approaching the goal (red) incurs a rapidly decreasing cost as it nears the goal while overshooting the goal incurs a disproportionately high cost almost immediately (Bischoff et al., 2013).

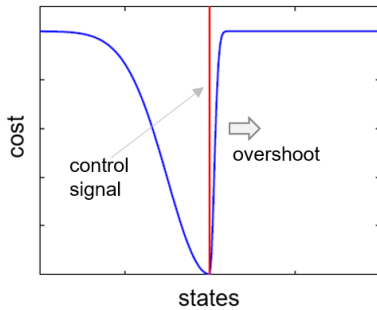


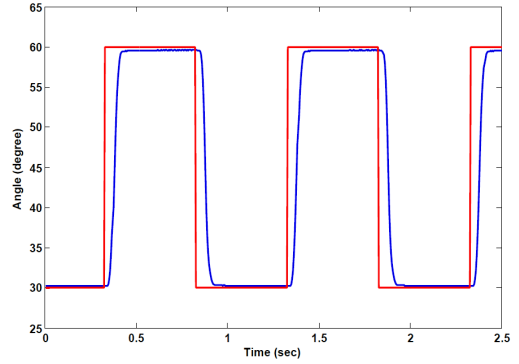
Figure 5: Asymmetric cost-function to avoid overshoots (Bischoff et al., 2013)

The effectiveness of the cost-function is evident in their results (blue) in Fig.6, with no overshoot and only a low-noise behavior of the controlled profile.

3.3.2. Heating, ventilation and air-conditioning (HVAC) control

Wang et. al (2018) use a model-free, proximal actor-critic based RL algorithm to control the nonlinear dynamics of HVAC systems where the hot-water flow is governed by a 3^{rd} power equation (10).

$$f_w(t) = 0.008 + 0.00703(-41.29 + 0.309u - 0.368 \times 10^{-4}u^2 + 9.56 \times 10^{-8}u^3) \quad (10)$$



(a) Control profile



(b) Zoomed section shows minor aberrations

Figure 6: Throttle valve control using PILCO (Bischoff et al., 2013)

RL is compared to Proportional-Integral (PI) and Linear Quadratic Regulator (LQR) control strategies. 150 time-steps are used to allow sufficient time for RL controller to learn tracking the set-point. Disturbances are simulated using random-walk algorithm. Actor network configuration is [50, 50] and the critic is a single layer of 50 units. One interesting aspect of the network architecture they employ is the use of GRU (Gated Recurrent Unit) to overcome the problem of vanishing/exploding gradients.

Fig.7 shows that the RL controller responds much faster than the LQR and PI controllers and tracks the reference signal better with lower integral-absolute and integral-square errors. However the RL shows a very high-variance noisy response against the smooth trajectories of PI and LQR controllers. Significant overshoots are also seen in the RL response.

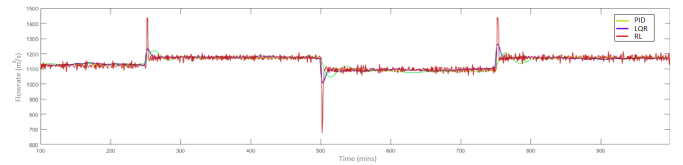


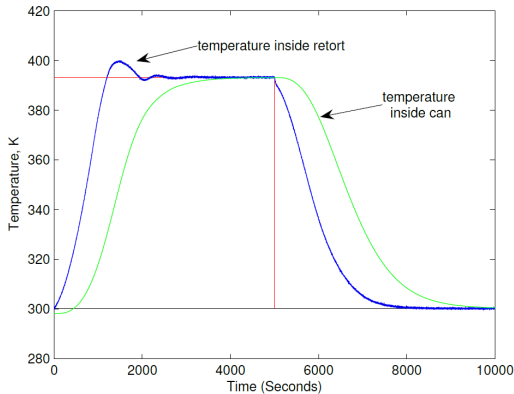
Figure 7: HVAC control (Wang et al., 2018)

3.3.3. Sterilization of canned food

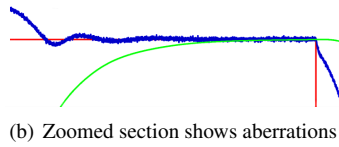
Thermal processing used for sterilization of canned food results in deterioration of the organoleptic properties of the food. Controlling the thermal process is therefore important. Syafie et al. (2008) apply Q-learning to learn the optimal temperature profile that can be applied during the two stages of the thermal process — manipulation of the saturated-steam valve to cause heating and then cooling by opening the water valve.

A simple *scalar* reward is used [+1.0, 0.0, -2.0], therefore penalizing an action deviating from the desired start twice

as more as rewarding it. The paper does not evaluate continuous rewards. Fig.8 shows the controlled temperature profile.



(a) Control profile



(b) Zoomed section shows aberrations

Figure 8: Thermal process control using Q-learning (Syafie et al., 2008)

Overall observations on the three researched papers:

1. Disturbances in the RL controlled signal are evident in all three implementations; (Bischoff et al., 2013), (Wang et al., 2018) and (Syafie et al., 2008).
2. Use of stochasticity mechanisms other than OUP to enable exploration of action space; (Bischoff et al., 2013) and (Wang et al., 2018).
3. Use of a novel objective function in (Bischoff et al., 2013).
4. *None* of these evaluated the stability of the RL controller design — an important consideration for an emerging breed of controllers.
5. MATLAB was not used for RL design³.
6. Only Wang et al. (2018) compared the RL against the traditional PID.

4. Experimental Setup

This section describes the creation of the experimental setup, using MATLAB and Simulink, for design and evaluation of the RL and PID controllers. Fig.9 shows the core components.

Our setup used elements from the excellent 2018 paper, “An augmented PID control structure to compensate valve stiction” by di Capaci and Scali.

Traditional PID controllers tuned solely on process dynamics, cause sustained oscillations attributed to the integral component that causes excessive variation of the control action to

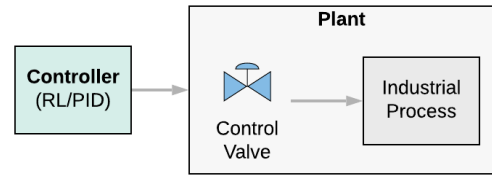
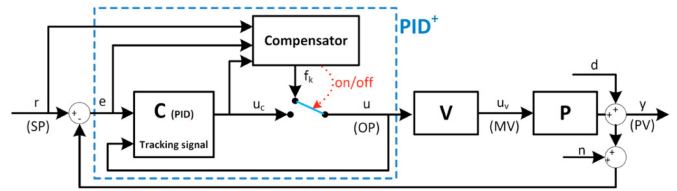
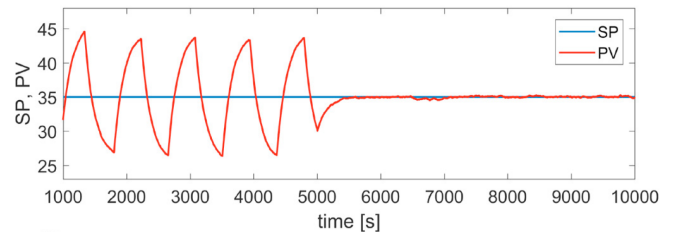


Figure 9: Basic block components

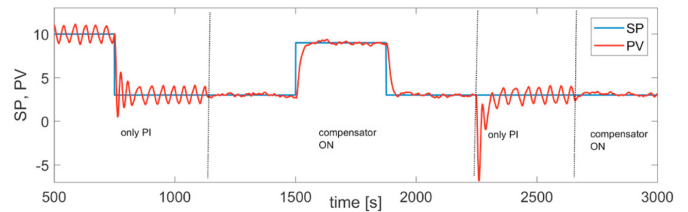
overcome static friction (di Capaci and Scali, 2018). As a solution to this di Capaci and Scali (2018) presented a novel PID based controller, Fig.10(a), where stiction is overcome by employing a *two-move control sequence* (11) as the valve input.



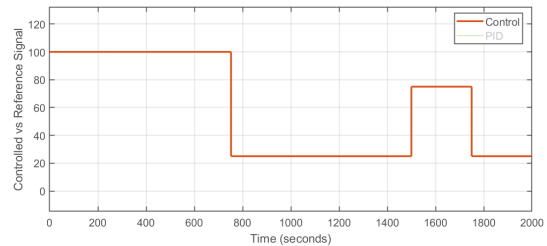
(a) Two-move compensator



(b) Compensator results on a constant reference signal



(c) Compensator results on a process with loop perturbations



(d) Regenerated “benchmark waveform”

Figure 10: “PID compensator” by di Capaci and Scali (2018)

³MATLAB launched the Reinforcement Learning Toolbox™ in Mar. 2019 (MathWorks, 2019a)

$$\begin{aligned}
u_k &= \begin{cases} u_{k-1} + a\hat{f}_S, & \text{if } u_{k-1} \geq \hat{x}_{ss} \\ u_{k-1} - a\hat{f}_S, & \text{if } u_{k-1} < \hat{x}_{ss} \end{cases} \\
u_{k+1} &= \begin{cases} \hat{x}_{ss} - \hat{f}_D, & \text{if } u_k \geq \hat{x}_{ss} \\ \hat{x}_{ss} + \hat{f}_D, & \text{if } u_k < \hat{x}_{ss} \end{cases} \\
u_{k+j} &= u_{k+1} (= u_{ss}), \text{ if } j > 1
\end{aligned} \tag{11}$$

where \hat{f}_S and \hat{f}_D are estimates of stiction and dynamic friction and \hat{x}_{ss} is the estimate of steady-state position of the valve. Equation (11) is highly dependent on the accurate estimations of friction parameters.

The setup components:

1. A PID (with filter) controller tuned using MATLAB's auto-tuning feature.
2. A training setup for the RL agent using the DDPG algorithm.
3. A unified framework for experimentation and evaluation of controllers

Items below were based on (di Capaci and Scali, 2018):

4. Nonlinear valve model (11) including the valve friction values f_S and f_D .
5. Two industrial processes controlled by the valve:
 - (a) Normal process (13).
 - (b) Process with loop perturbations (22).
6. A "benchmark waveform" profile with noise parameters (Fig.10(d)).

4.1. Modeling the valve

Simscape Fluids™ provides simulations for several valve types and is the simplest and quickest option. (Popinchalk, 2006) is a MathWorks article to enhance these into more realistic models using an understanding of system dynamics.

We use first-principles and mathematically model the non-linear valve. Algebraically rearranging equations shown in (11) produces (12); these equations are then implemented in Simulink using code in a "user-defined-function" (Listing.1) and a "memory" block shown in Fig.11 with $f_S = 8.40$ and $f_D = 3.524$.

$$x_k = \begin{cases} u_k - f_D, & \text{if } u_k - x_{k-1} > f_S \\ u_k + f_D, & \text{if } u_k - x_{k-1} < -f_S \\ x_{k-1}, & \text{if } |u_k - x_{k-1}| \leq f_S \end{cases} \tag{12}$$

Listing 1: MATLAB script for modelling a non-linear valve

```

function xk = fcn(fD, fS, uk, xkp)
t_xk = 0.0;
if ((uk-xkp) > fS)
    t_xk = uk - fD;
elseif ((uk-xkp) < -1*fS)
    t_xk = uk + fD;
elseif (abs(uk-xkp) < fS)
    t_xk = xkp;

```

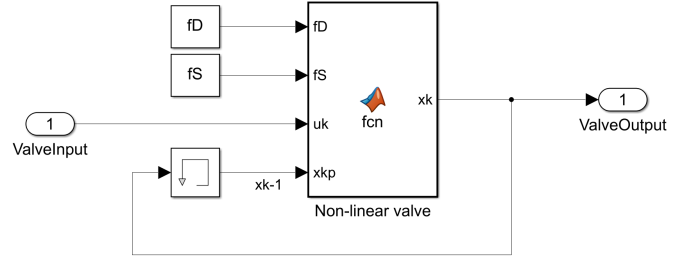


Figure 11: Simulink valve model

end

```

% Return the valve output
xk = t_xk;

```

4.2. Modeling the "industrial" process

The benchmark "industrial process" is modeled as a first-order plus time-delay (FOPTD) process (13), using transfer-function and time-delay blocks as shown in Fig.12.

$$G(s) = \frac{k}{(1 + Ts)} e^{-Ls}, \tag{13}$$

where $k = 3.8163$, $T = 156.46$ and $L = -2.5$.

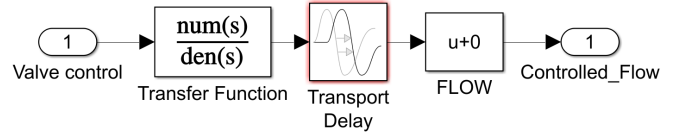


Figure 12: FOPTD process model

4.3. PID controller setup

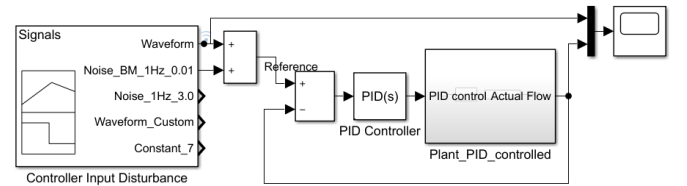


Figure 13: PID control setup

A PID controlled output is a function of the feedback error, represented in time-domain as:

$$u(t) = K_p e + K_i \int e(t).dt + K_d \frac{de}{dt} \tag{14}$$

where u is the desired control signal and $e(t) = r(t) - y(t)$ is the tracking error, between the desired output r and the actual output y . This error signal is fed to the PID controller, and the controller computes both the derivative and the integral of this

error signal with respect to time providing a set-point tracking effect, this works continuously in a closed loop, until the controller is in effect.

The ideal theoretical PID form exhibits a drawback for high frequency signals — the derivative action results in very high gain. A high frequency measurement noise will therefore generate large variations in the control signal. Practical implementations reduce this effect by replacing the K_d term by a first-order filter (where $K_d.de/dt$ is represented as $K_d.s$ in Laplace form) by (15) (Murray et al., 1994).

$$K_p + K_i \frac{1}{s} + K_d \frac{N}{(1 + N\frac{1}{s})} \quad (15)$$

The filter coefficient N determines the pole location of the filter that helps attenuate the high gain on high-frequency noise. A N between 2 and 20 is recommended. A high value ($N > 100$) results in (15) approaching the ideal form (14) (Murray et al., 1994).

The PID was tuned using MATLAB auto-tuning feature and the coefficients obtained were $K_p = 0.3631$, $K_i = 0.0045$, $K_d = -1.72$ and $N = 0.0114$. The low N acts to suppress the derivative term.

4.4. RL controller setup

Fig.14 shows the Simulink setup, for training *and* evaluation of the RL controller.

Training an agent involves significant hyperparameter tuning and a switch allowed for quick experiments with numerous signals fed via a “signal-builder” block.

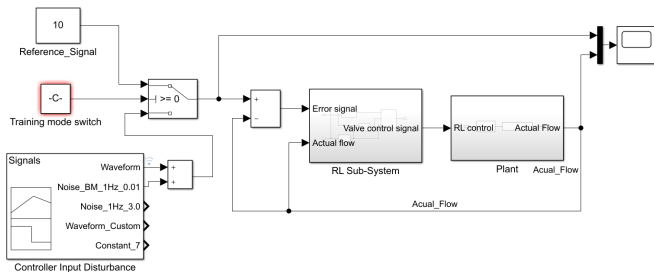


Figure 14: RL agent training setup

4.4.1. RL controller design

Fig.15 shows the DDPG Agent block with feedback from the environment channelized via the Observations vector. It also shows the block that computes Rewards and the Stop-simulation block that controls the termination of an episode.

4.4.2. Environment design

Several design factors need consideration, when building the environment, for efficiently training an agent to follow trajectories of a control signal. They can broadly be classified into agent related and environment related.

Agent related factors are composition of the observations vector and the reward strategy. Environment related factors cover the training strategy, training signals, initial conditions of the environment and criteria to terminate an episode.

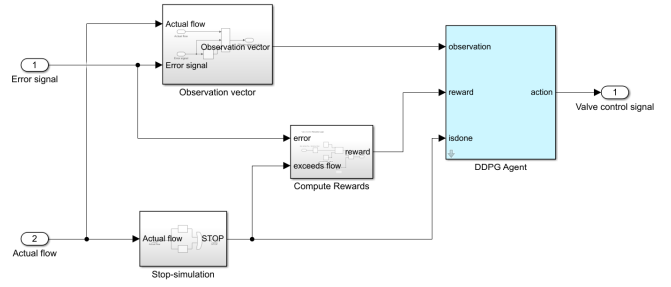


Figure 15: RL DDPG agent details

4.4.3. Training strategy

One could train the RL agent to follow the exact benchmark trajectory (Fig.10(d)), however this is a very constrained strategy. Instead, the agent was trained to follow random levels of straight-line (constant) signals. The agent was additionally challenged to learn to start at a randomly initialized flow value. Together this forms an effective and generalized training strategy to teach the agent to follow *any* control signal trajectory composed of straight lines. The RL ToolBox allows overriding the default “reset function” that assists in implementing the above strategy.

```
env.ResetFcn = @(in)localResetFcn(in,
    VALVE_SIMULATION_MODEL);
```

4.4.4. Observation vector

The observation vector, modeled as shown in Fig.17, is composed of: $[y; e; \int e.dt]^T$, where y is the actual flow achieved, e the error with respect to reference r , and finally the integral of the error.

Integral of error: The instantaneous error has no memory. The integral of error, which is the area under the curve as time progresses, provides a mechanism to compute the total error gathered over time and drive the agent to lower this (Fig.16). This is an important observation input often used in training of RL controllers.

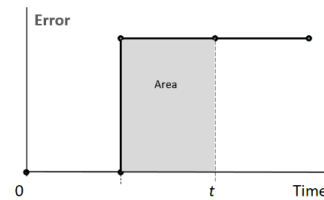


Figure 16: Error integral

4.4.5. Rewards strategy

Rewards can be assigned via discrete, continuous or hybrid functions. Equation (16) is a simple discrete form.

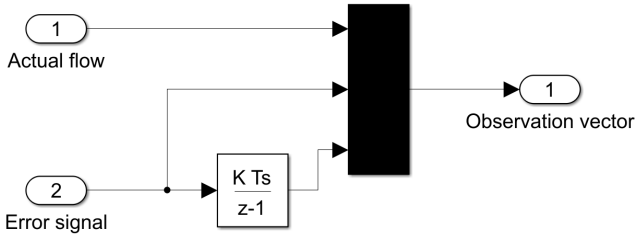


Figure 17: RL observations vector

$$Reward = \begin{cases} 10, & \text{if } |e| < \Delta \\ -1, & \text{if } |e| \geq \Delta \\ -100, & \text{if } (y \leq 0, y > Max_Flow), \end{cases} \quad (16)$$

where Δ is some allowable error margin.

Equation (17) shows a reward that varies continuously as a function of error e . λ is a small constant that avoids division-by-zero error.

$$Reward = \begin{cases} -100, & \text{if } (y \leq 0, y > Max_Flow) \\ \frac{1}{(e+\lambda)}, & \text{otherwise} \end{cases} \quad (17)$$

Fig.18 shows the final implementation as a hybrid form. The reciprocal of the absolute error allows the controller to learn to drive the error lower and lower. The discrete part of the reward is the “penalty” block that assigns a set penalty for exceeding the flow limits.

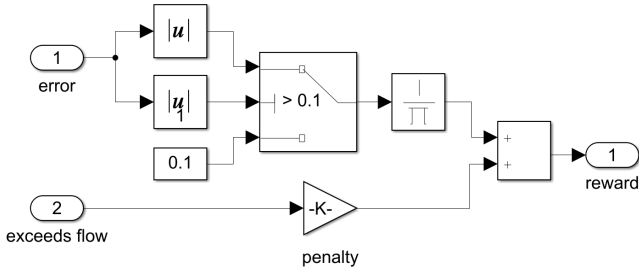


Figure 18: RL rewards computation block

4.4.6. Actor and Critic networks

The actor-critic DDPG components were implemented as shown in Fig.19. The networks have fully-connected layers, initialized with small random weights before beginning the training.

The actor network output is normalized to be between $[-1, 1]$ using a \tanh layer. This allows better learning and convergence for continuous action spaces.

4.4.7. Ornstein-Uhlenbeck (OU) action noise parameters

(MathWorks, 2019b) provides guidelines for computing the DDPG exploration parameters — noise model variance and its decay rate via (18).

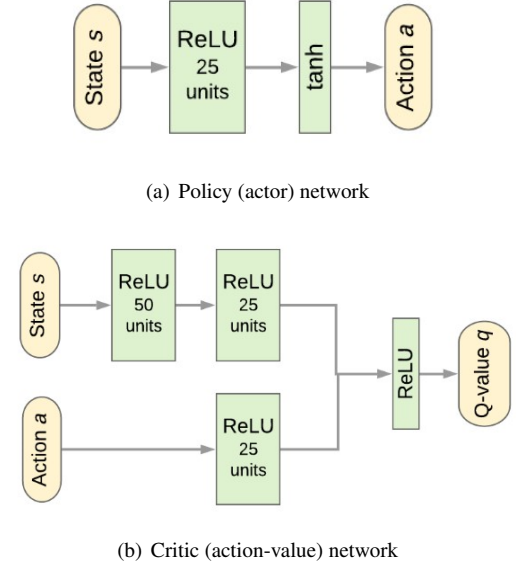


Figure 19: DDPG network architectures

$$Variance. \sqrt{T_s} = (1\% \text{ to } 10\%) \text{ of } ActionRange \quad (18)$$

where T_s is the sampling time

On deciding a half-life of the variance factor, in time-steps, the decay rate is then computed using (19)

$$HalfLife = \frac{\log(\frac{1}{2})}{\log(1 - VarianceDecayRate)} \quad (19)$$

4.4.8. Final DDPG hyperparameters

Table 1 summarizes the final set of DDPG hyperparameters.

Table 1: DDPG hyperparameter settings

Hyperparameter	Setting
Critic learning rate	$1e^{-03}$
Actor learning rate	$1e^{-04}$
Critic hidden layer-1	50 fully-connected
Critic hidden layer-2	25 fully-connected
Action-path neurons	25 fully-connected
Action-path bound	\tanh layer
Gamma	0.9
Batch size	64
OUP Variance	1.5
OUP Variance Decay Rate	$1e^{-05}$

4.5. Setup for comparative study

An environment that combines the PID and RL strategies for a comparative evaluation is shown in Fig.20. It allows experimenting with various reference signals, studying the effects of noise added at three disturbance points i.e. input of the controller, output of the controller (i.e. the input of the plant) and finally output of the plant.

It provides a convenient platform to perform additional experiments using elements such as set-point filters, output smoothing filters, etc.

5. Graded Learning

Before presenting the results of the experiments we elaborate on “Graded Learning”, a progressive *coaching method*. This simple, *intuition* based approach was discovered *accidentally* during the hundreds of experiments and trials (163 to be exact) that were conducted in an attempt to train a stable RL agent. It must be noted that this method, though discovered inadvertently, is equivalent to the naive, domain-expert dependent form of the more formal method known as “Curriculum Learning” (Weng, 2020; Narvekar et al., 2020).

Applying automatic Curriculum Learning requires algorithmic design and implementing complex frameworks (Portelas et al., 2019), for example ALP-GMM (absolute learning progress Gaussian mixture model) “teacher-student” frameworks. The “teacher” neural-network samples parameters from the continuous action space to generate a learning curriculum. Applying automated Curriculum Learning is not readily available as a feature in MATLAB; Graded Learning, on the other hand, requires no programming and can be easily implemented by a control engineer.

Fig.21 shows examples of the numerous challenges faced during training, sometimes resulting in experiments with thousands of episodes that did not produce a stable learning curve and sometimes resulting in inexplicable controller actions. Some training trials lasted 20,000 episodes running for over 20 hours and therefore it is important to streamline these efforts.

Graded Learning helped avoid some of these challenges. The intuition for Graded Learning was based on observing how human instructors structure *coaching* of a new skill for apprentices.

While new skills such as chess or tennis are taught with the final goal in mind, one never starts with the hardest lessons. Foundation level skills are taught first and once some level of proficiency is gained, the student graduates to the next level to handle marginally more complex problems. Skills and experiences gained at any level are retained and progressively built upon while moving to higher levels.

Graded Learning extends this iterative staged approach to RL. The RL task is first broken down to its fundamental level, an agent is trained for n episodes or until convergence criteria is met. Next level of complexity is added to the previous task. *Transfer-learning* is used to ensure previous experiences are retained and built upon. Once this level of task is learned, the process of adding further complexity continues and each time

transfer-learning allows to build upon experience gained during the previous levels.

Transfer-learning is a machine learning technique that is used to “transfer” the learning i.e. stabilized weights of a neural-network from one task (or domain in general) to another without having to train the neural-network from scratch (Weiss et al., 2016).

The Graded Learning approach was discovered when the time-delay in (13) was reduced to zero and the agent quickly stabilized in contrast to the hundreds of earlier attempts.

Fig.22 demonstrates the method in action and the agent evolving over six stages of *increasing difficulty*. Parameters that are progressively increased are: time-delay L , static friction f_s and dynamic friction f_D .

The stability analysis and experimental results presented next, demonstrate that Graded Learning applied to valve control (and possibly other complex industrial systems) appears to be an effective way to coach an RL agent.

6. Experiments, Results and Discussion

In this section we present the results of experiments conducted to evaluate the RL controller’s performance and compare it with the PID (with filter) controller.

Before conducting the experiments a stability analysis of the RL controller must be carried out.

6.1. Stability Analysis of RL Control

A basic stability analysis of the RL control is attempted in this section.

Open-loop transfer-function of the system is $C(s) \cdot P(s)$. Transfer-function of the plant $P(s) = V(s) \cdot G(s)$ where $G(s)$ is the transfer-function of the FOPTD process (13) and $V(s)$ is the transfer-function of the nonlinear valve which is unknown and must be estimated.

Simulink’s Control Design Linearization Analysis™ tool provides a GUI based interface to generate a *linear approximation* of a nonlinear system, computed across specified input and output points. However, this does not allow any control over the estimation in contrast to MATLAB’s `tfest` function.

The programmatic method allows a user to estimate the transfer-function by specifying the number of poles (`np`) and zeros (`nz`). Additionally the `iodelay` parameter allows experimenting the effect of time-delays in physical systems. This MATLAB function is based on (Garnier et al., 2003).

```
sys = tfest(data, np, nz, iodelay)
```

The block-diagram Fig.23 shows the points at which data u_1 and y_1 will be tapped to estimate the controller transfer-function $C(s)$ and points u_2 and y_2 to estimate the complete plant transfer-function $P(s)$. Fig.24 is the Simulink setup to assist in estimation.

Estimated transfer-functions: The estimated continuous-time transfer-function for the plant is (20), with a fit of 97.15% and MSE of 0.7921, while that of the controller is (21).

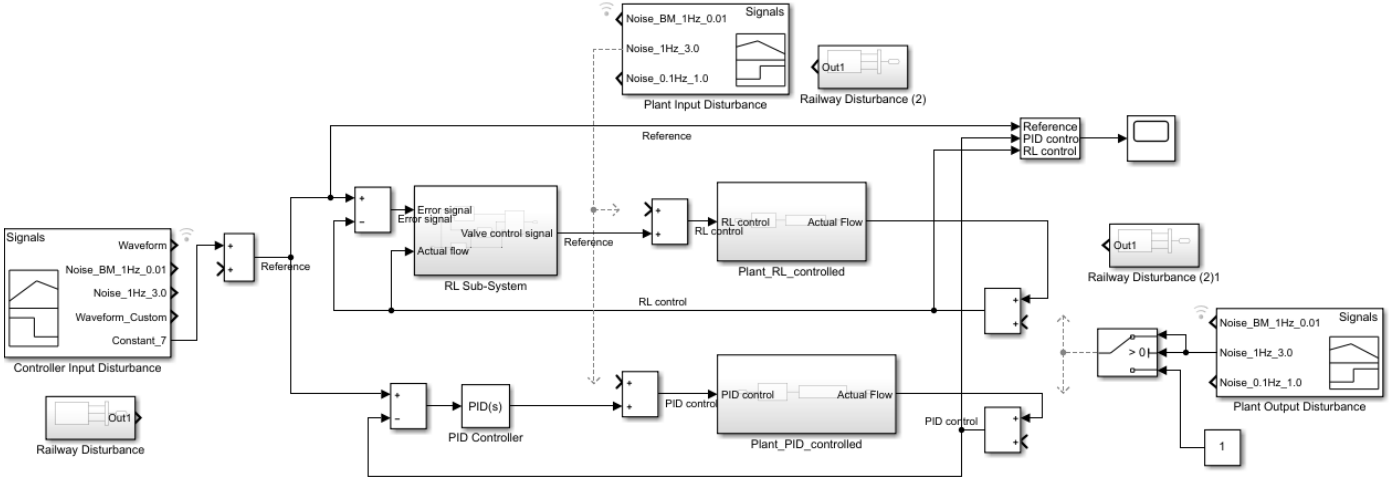


Figure 20: Unified setup for a comparative evaluation of RL and PID control strategies

Table 2: Graded Learning: Staged learning parameters and training times

Grade	L	f_s	f_D	Episodes	Time (h)
Grade-I.1	0.1	$\frac{1}{10} \times 8.4$	$\frac{1}{10} \times 3.524$	930	1.67
Grade-I.2	0.1	$\frac{1}{10} \times 8.4$	$\frac{1}{10} \times 3.524$	2000	12.35
Grade-II	0.5	$\frac{1}{5} \times 8.4$	$\frac{1}{5} \times 3.524$	1000	5.31
Grade-III	1.5	$\frac{1}{2} \times 8.4$	$\frac{1}{2} \times 3.524$	1000	5.21
Grade-IV	1.5	$\frac{2}{3} \times 8.4$	$\frac{2}{3} \times 3.524$	1000	4.65
Grade-V	2.0	$\frac{2}{3} \times 8.4$	$\frac{2}{3} \times 3.524$	500	2.27
Grade-VI	2.5	8.4	3.524	2000	7.59
Total				8430	39.05

$$\frac{0.002255s^2 - 1.904 \times 10^{-5}s + 8.563 \times 10^{-7}}{s^3 + 0.01305s^2 + 9.451 \times 10^{-5}s + 2.278 \times 10^{-7}} \quad (20)$$

$$\frac{0.09455s^2 + 0.0005729s + 1.609 \times 10^{-6}}{s^3 + 0.2312s^2 + 0.001939s + 1.195 \times 10^{-7}} \quad (21)$$

We plot (Fig.25), the plant's response using the estimated transfer-functions against the actual response; to ensure that the estimations are reasonable for conducting a basic stability analysis.

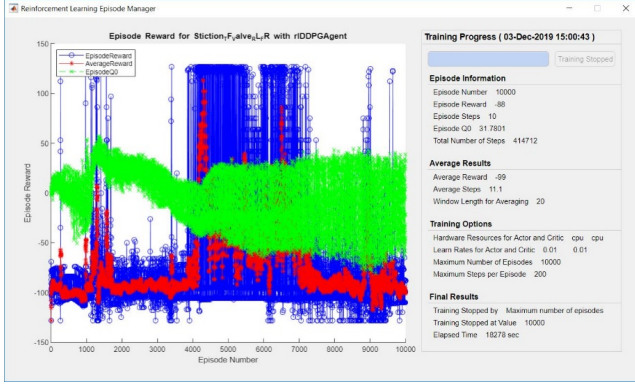
Stability analysis: The step-response in Fig.26 shows a stable closed-loop system. The open-loop Bode plot, Fig.27, shows a gain-margin of 10.9 dB and a phase-margin of 68.0 degrees, indicating a fairly stable system.

6.2. Experiments and Results

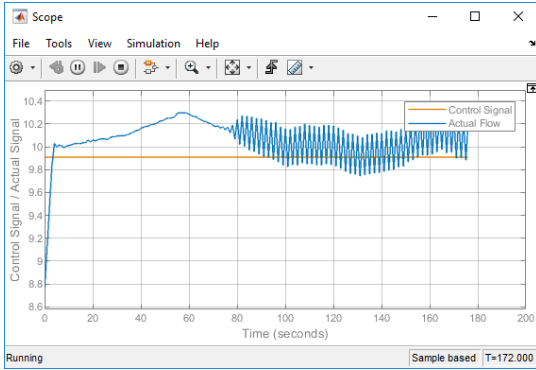
In this section we present the results of experiments conducted on a unified framework that tests two valve control strategies — PID (with filter) and DDPG RL. A critical time-domain analysis of experiments with varying control signals, varying noise strengths and disturbance points and effect of a plant with process-loop perturbations is presented.

Experiments conducted:

1. Arbitrarily assumed constant reference level.
2. Benchmark waveform (with noise).
3. Benchmark waveform subject to disturbances at:
 - Controller input (i.e. reference signal).
 - Plant input (i.e. controlled signal fed to plant).
 - Plant output (i.e. system output).



(a) Inexplicable learning curves



(b) Inexplicable controller actions

Figure 21: RL agent: Indicative training challenges from our trials

4. Practical example of a “water-supply” valve, subject to ground-borne vibrations of passing trains.
5. Plant experiencing process loop-perturbations.
6. Arbitrary control waveform.

6.2.1. Experiment-1: Constant reference signal

Experiment: A basic analysis is best done on a simple constant reference flow rate arbitrarily set at 100 and run over 2,000 s. Reference signal is superimposed with benchmark Gaussian noise ($\mu = 0.0, \sigma = 0.01$).

Observations: In Fig.28 the PID shows a large overshoot and settles in about 700 s. The RL strategy demonstrates close to ideal damping and a quicker settling time of about 220 s. The RL trajectory shows tiny ripples against the PID’s smoother profile. These oscillations can reduce the remaining-useful-life (RUL) of a mechanical system and we study this by conducting a (simplified) two factor DOE (design of experiments).

We vary the two factors; time-delay and valve friction (combined static and dynamic) as shown in Table 3. The default values of time-delay $L = 2.5$, static-friction $f_s = 8.40$ and $f_D = 3.524$ are treated as the high-levels and we lower each by a factor of 100 to obtain the low-levels as shown in Table 4.

Table 3: DoE table

Time-delay (L)	Friction values (f_s, f_D)
Low	Low
Low	High
High	Low
High	High

Table 4: DoE table with actual values

L	f_s	f_D
0.025	0.084	0.0352
0.025	8.400	3.524
2.500	0.084	0.0352
2.500	8.400	3.524

Fig.29(a) highlights the RL’s capability to produce a very smooth profile when both the factors are low. This implies that the oscillations are not introduced by the RL technique. Fig.29(c) shows that the cause of oscillatory behavior is mainly due to the time-delay factor.

While the PID strategy (15), is implemented with a filter that suppresses noise, *no* filters were added to the RL setup to better understand the natural response of RL control strategies.

6.2.2. Experiment-2: The benchmark signal

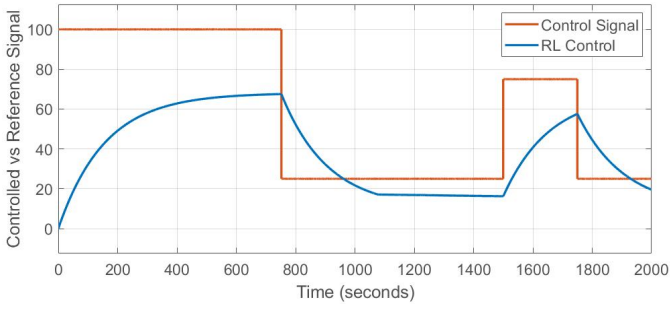
Experiment: The waveform profile used in (di Capaci and Scali, 2018), with Gaussian noise ($\mu = 0.0, \sigma = 0.01$), is subject to both strategies. We also zoom sections of time-domain plot Fig.30 and observe them more closely in Fig.31.

It is observed that PID shows higher over- and under-shoots. If such a valve controls fluid flow, the higher and lower fluid quantities could be detrimental to the product quality. In 30 the shifted PID waveform after 800 s could be detrimental to the process if it depends on the timing of the flow of fluid. In contrast RL control shows better tracking of reference signal.

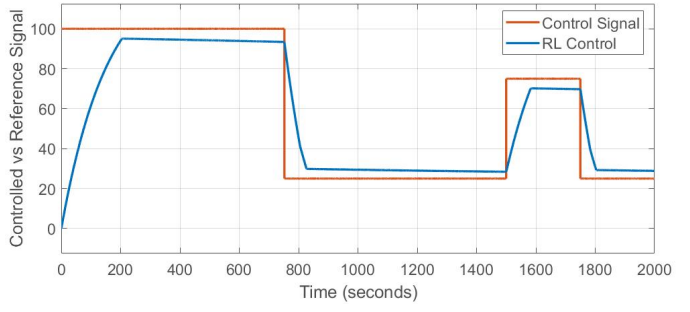
6.2.3. Experiment-3.a: Noise at controller input

Experiment: Increase noise at the controller input ($\mu = 0, \sigma = 3.0, 1Hz$)

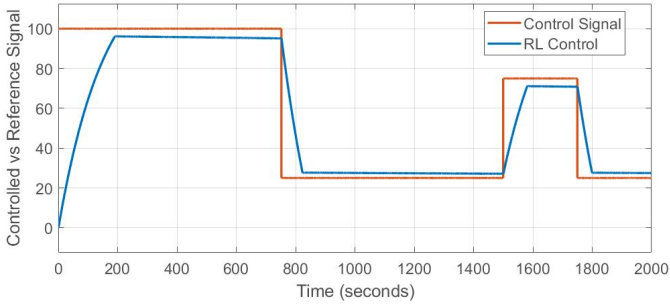
Observations: Fig.32(a) and 32(b) show almost no impact on the PID when compared with Experiment-2 (lower noise at input) but increased impact on the RL trajectory, demonstrating the PID strategy’s superior noise attenuation capabilities. The RL continues to closely track the reference signal (*along* with the noise).



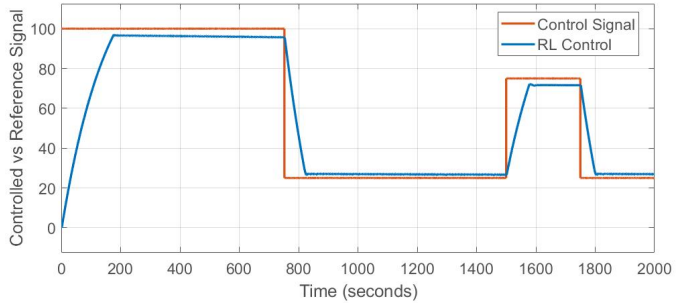
(a) Grade-I: $L=0.1$, $f_S = \frac{1}{10} \times 8.4$, $f_D = \frac{1}{10} \times 3.524$



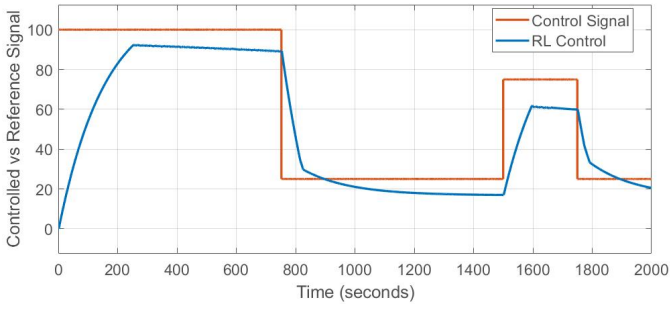
(b) Grade-I.2: *Grade-I* trained for a further 1000 episodes



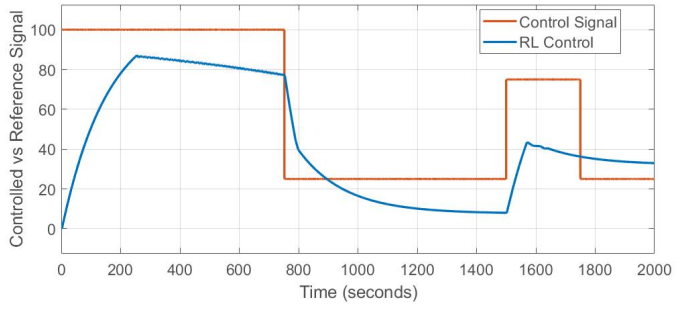
(c) Grade-II: $L=0.5$, $f_S = \frac{1}{5} \times 8.4$, $f_D = \frac{1}{5} \times 3.524$



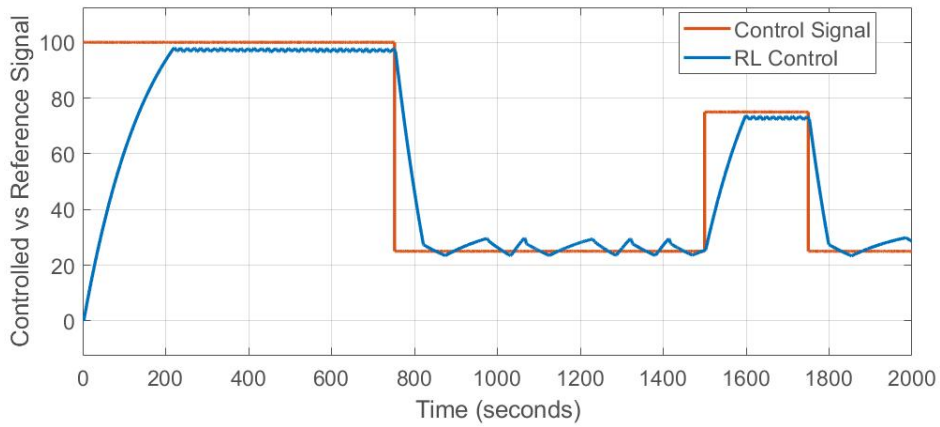
(d) Grade-III: $L=1.5$, $f_S = \frac{1}{2} \times 8.4$, $f_D = \frac{1}{2} \times 3.524$



(e) Grade-IV: $L=1.5$, $f_S = \frac{2}{3} \times 8.4$, $f_D = \frac{2}{3} \times 3.524$



(f) Grade-V: $L=2.0$, $f_S = \frac{2}{3} \times 8.4$, $f_D = \frac{2}{3} \times 3.524$



(g) Final learned model: Grade-VI: $L=2.5$, $f_S=8.4$, $f_D=3.524$

Figure 22: Graded Learning: Progressive learning of task

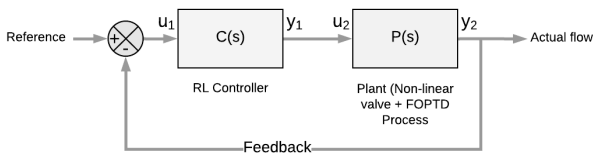


Figure 23: Block diagram of a single-loop control system

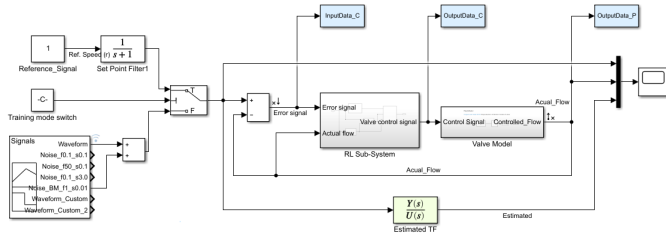


Figure 24: Setup for transfer-function estimation

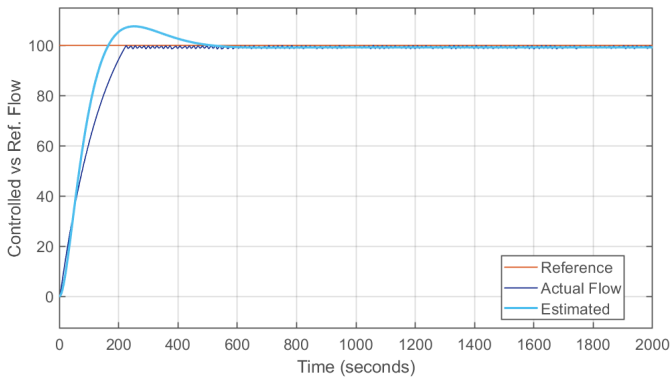


Figure 25: Stability analysis: Comparing plant responses using the estimated transfer-functions

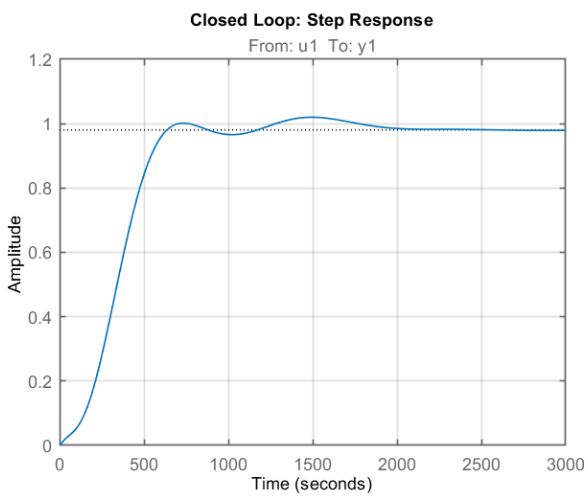


Figure 26: RL controller: Step response

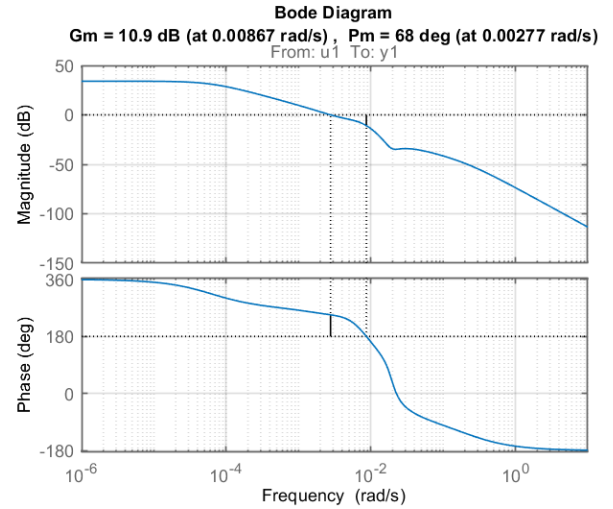


Figure 27: RL controller: Open-loop Bode loop

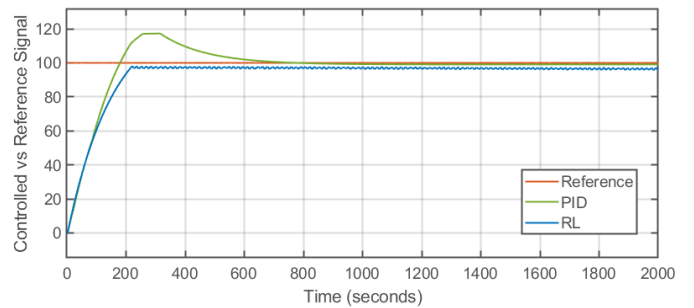


Figure 28: Expt.-1: Constant reference signal

6.2.4. Experiment-3.b: Noise at plant input

Experiment: Shift the source of noise to the plant input ($\mu = 0, \sigma = 3.0, 1Hz$).

Observations: Fig.33 shows that the PID trajectory is now impacted and it loses its relatively smooth output seen in Experiment-1 and Experiment-2. The RL strategy on the other hand remains *unaffected* when compared to Experiment-1. The PID strategy adjusts itself based on the error signal and hence shows a change in behavior while RL strategy does not.

6.2.5. Experiment-3.c: Noise at plant output

Experiment: Effect of noise at the plant output ($\mu = 0, \sigma = 3.0, 1Hz$).

Observations: Fig.34(a) shows that both RL and PID strategies are affected equally.

6.2.6. Experiment-4: Water-supply valve, subject to ground-borne vibrations

Experiment: Valve applications could often be exposed to extremely harsh conditions. A water-supply system, for example, may face ground-borne vibrations such as from passing railways, that is in the range of about 30–200 Hz and varying amplitudes (Southampton.ac.uk). Since the control-valve assembly will often be placed in shielded environments frequencies between 30–100 Hz were assumed for simulation.

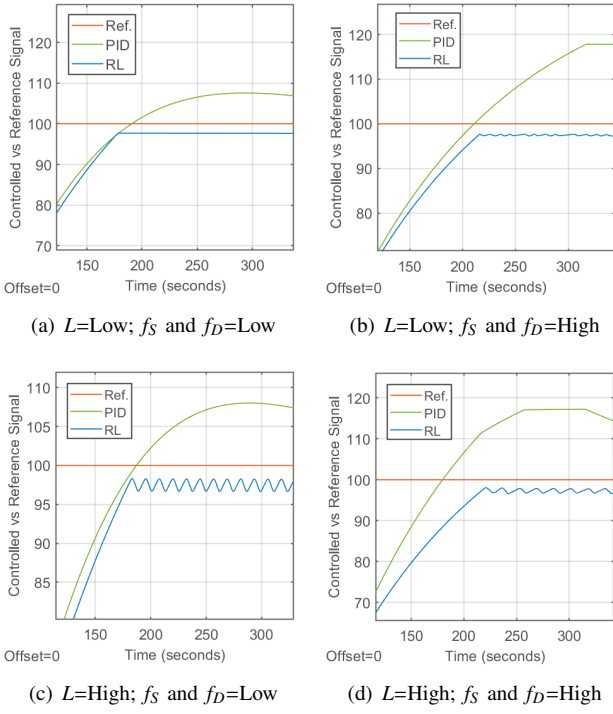


Figure 29: Expt.-1: DoE with time-delay and friction parameters

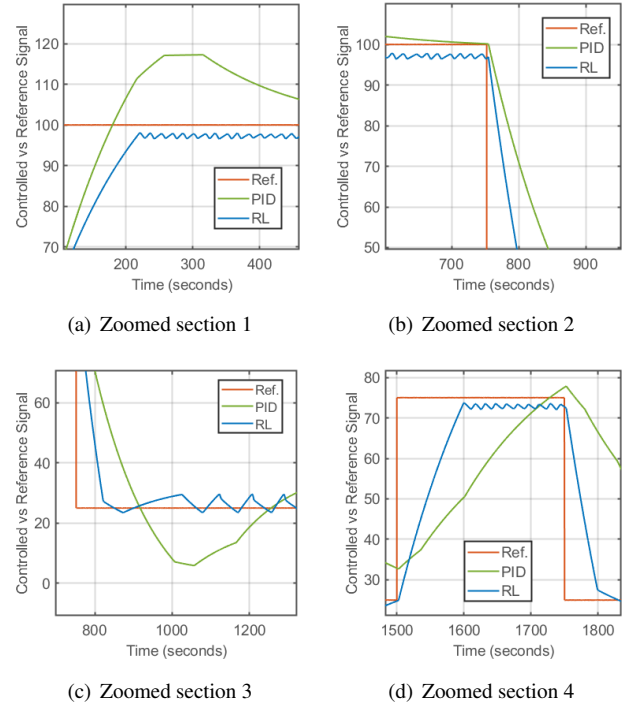


Figure 31: Expt.-2: Zoomed sections of the benchmark signal

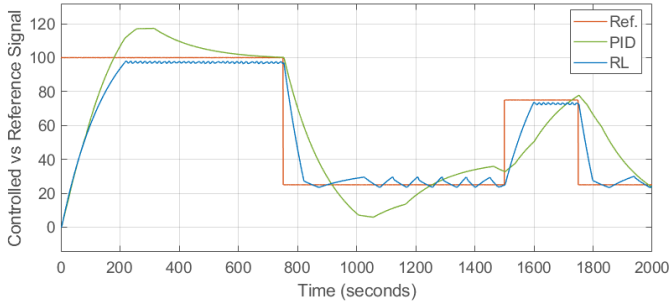
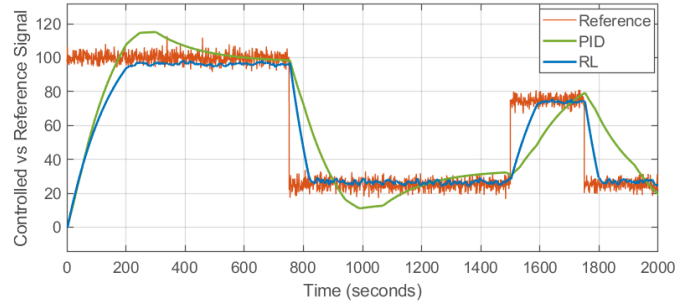
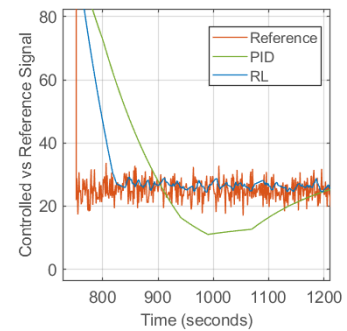


Figure 30: Expt.-2: Benchmark waveform



(a) Entire trajectory plot



(b) Zoomed section

Figure 32: Expt.-3.a: Noise at controller input ($\mu = 0, \sigma = 3.0, 1Hz$)

Observations: Figures 35(a) and 35(b) show that, as in Experiment-3.c, the impact of noise is similar on both strategies and RL continues to track the reference signal better than PID.

6.2.7. Experiment-5: Arbitrary control waveform with benchmark noise signal

Experiment: Test the generalization capability of RL training strategy vis-à-vis generalization of PID tuning. “Training” signal for both the strategies was the benchmark waveform and this experiment subjected them to a completely different waveform.

Observations: Fig.36 shows that the RL controller outperforms the PID strategy considerably in this experiment. The RL controller tracks the arbitrary reference more closely and this demonstrates the importance of the training strategy in effective generalization. The PID trajectory, on the other hand shows a significant lag while tracking the reference and if such

a valve controls fluid flow, the untimely higher or lower fluid quantities could be detrimental to the product quality.

Small ripples are evident in sections of the RL controlled trajectory.

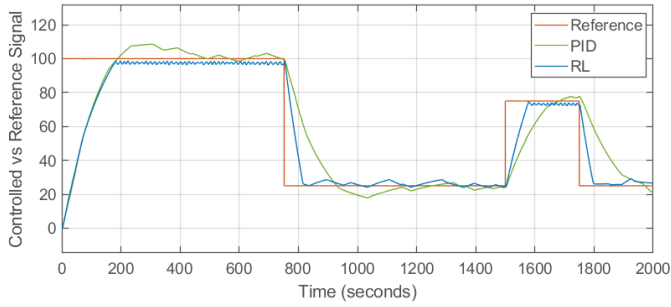
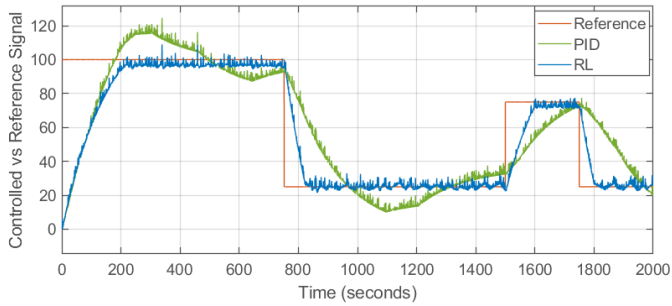
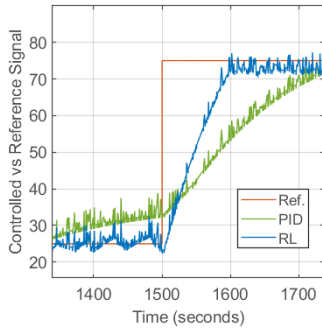


Figure 33: Expt.-3.b: Noise at plant input ($\mu = 0, \sigma = 3.0, 1Hz$)



(a) Entire trajectory plot



(b) Zoomed section

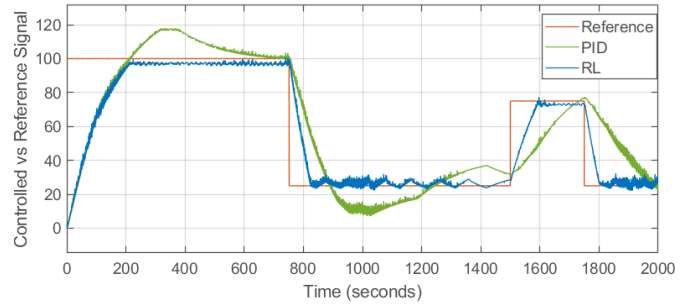
Figure 34: Expt-3c: Noise at plant output ($\mu = 0, \sigma = 3.0, 1Hz$)

6.2.8. Experiment-6: Benchmark plant with process loop perturbations

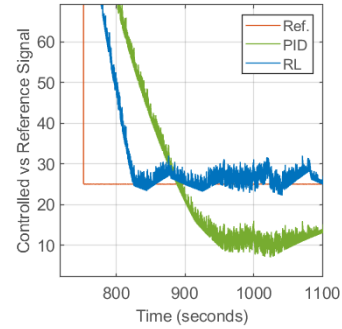
Experiment: Evaluate resistance to severe process-loop perturbations modeled as a 3rd order transfer-function (22) (di Capaci and Scali, 2018).

$$G(s) = \frac{1}{(1s + 1)(5s + 1)(10s + 1)} \quad (22)$$

Observations: A severe *limitation* of the RL controller is evident in this experiment. Fig.37 shows a significantly stunted output, clamped smoothly at around 35.0. The setup was then tested on a lower magnitude reference Fig.37(b) and the RL continues to be clamped at the same level, 35.0. PID seems to scale to different levels under the influence of perturbations albeit with significant error. The RL controller shows increased oscillatory behavior at the lower flow level.

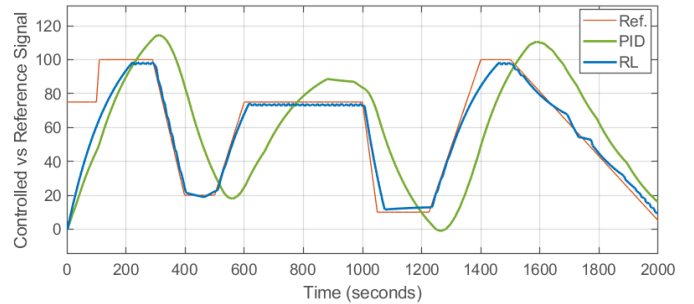


(a) Entire trajectory plot

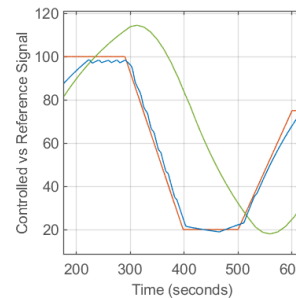


(b) Zoomed section

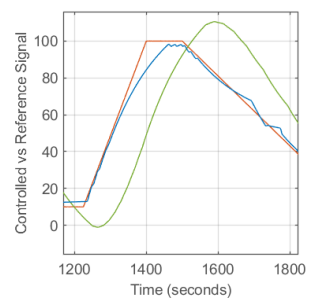
Figure 35: Expt.-4: Ground-borne vibrations of a passing train



(a) Arbitrary control waveform



(b) Zoomed section 1

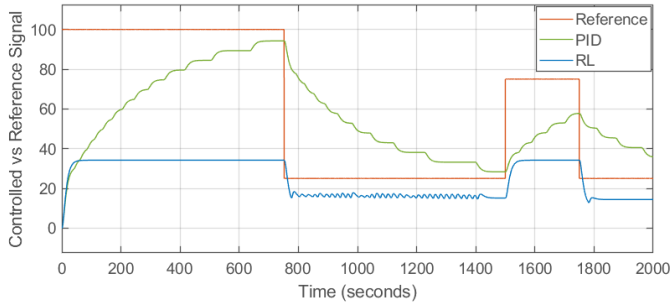


(c) Zoomed section 2

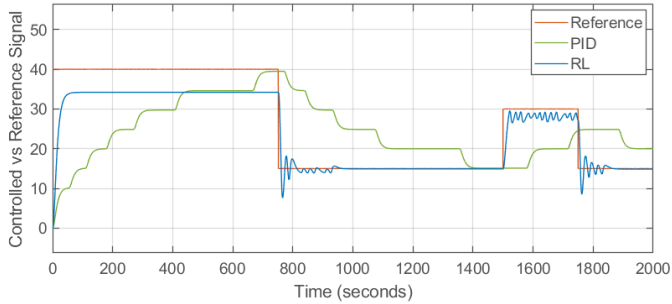
Figure 36: Expt.-5: Response to an arbitrary control waveform

6.3. Discussion: Experiential Learning Validated against Published Research

Merriam-Webster: “Experiential: relating to, *derived from*, or providing *experience*”



(a) Response to benchmark signal



(b) Response to benchmark signal with lower strength

Figure 37: Expt.-6: Response to plant with perturbations

A total of 163 experiments were conducted during this research. When experiments did not respond to seemingly logical steps it led to severe frustration. In a quest to find answers for some of the strange observations, research was conducted to relate these to previously published studies and it highlighted the several known challenges that exist; reminding one that RL is still an emerging field.

Early adopters of RL for control are encouraged to try both the Graded Learning method and study the literature referenced in this section — which is a collection of studies conducted at Google, MIT and Berkeley; (Song et al., 2019; Henderson et al., 2017; Hardt et al., 2015; Zhang et al., 2018).

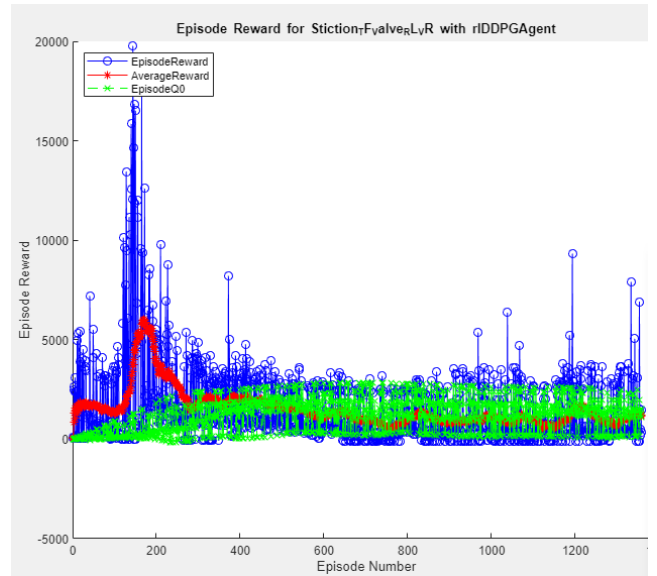
In (Henderson et al., 2017), effects of hyperparameters and their tuning are analyzed with respect to network-architecture, rewards scaling and reproducibility on model-free, policy-gradient based algorithms for continuous control and is therefore directly applicable to the subject of this paper.

6.3.1. Over-fitting and saturation

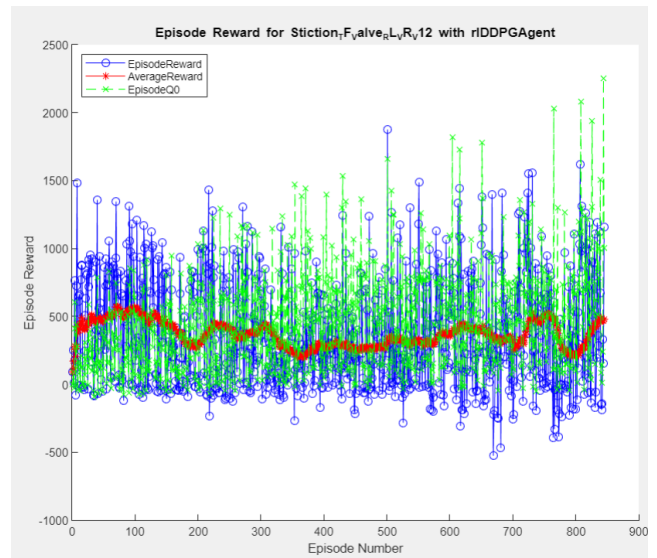
For physical systems, there is always an upper limit of performance that the agent cannot surpass. However this is not known before hand and one often pushes the agent to continue training for hours. Significant neural-network saturation was observed in several of the training attempts, Fig.38.

Over-fitting in RL is being studied only recently. Song et al. (2019) observe that in model-free RL, the agent often mistakenly correlates rewards with spurious observation-space features (“observational overfitting”). In particular they have studied over-fitting with linear quadratic regulators (LQR) using neural-networks and show that under Gaussian initialization of

the policy using gradient descent, a generalization gap “must necessarily exist”.



(a) Example-1



(b) Example-2

Figure 38: Examples from our trials showing effects of over-training and network saturation

Hardt et al. (2015) provides a theoretical proof, that stochastic-gradient methods employing parametric models, when trained using *fewer* iterations, have vanishing generalization errors. They argue this by experiments conducted and using stability criteria established for learning algorithms devised by Bousquet and Elisseeff. They conclude, that shortened training time by itself, sufficiently prevents over-fitting. This paper is important for extending the stability criteria developed for supervised learning to iterative algorithms, such as RL (Bousquet and Elisseeff, 2002).

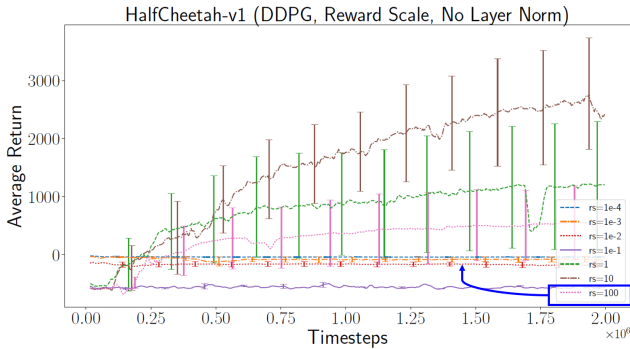
6.3.2. Sensitivity to network architecture

Four policy-gradient methods including the DDPG are analyzed in (Henderson et al., 2017). While ReLU activations were stated to perform best, the effects were not consistent across algorithms or hyperparameter settings.

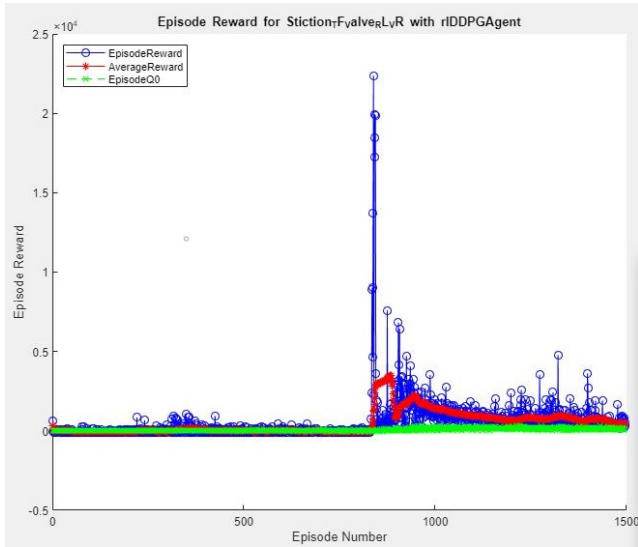
6.3.3. Sensitivity to reward-scaling

A large and sparse reward scale causes network saturation; resulting in inefficient learning. Reward rescaling is a technique recommended to improve results for DDPG. This is achieved by multiplying by a scalar such as 0.1 or clipping to $[0, 1]$ (Duan et al., 2016).

Fig.39(a) shows the effects of different reward scales conducted by Henderson et al. (2017); with 10^2 highlighted for comparison with similar scales, observed in trials we conducted (Fig.39(b)). Reward scale can exhibit a large impact and must be given due consideration (Henderson et al., 2017).



(a) Published results (Henderson et al., 2017)



(b) Inefficient learning at 10^2 reward scales

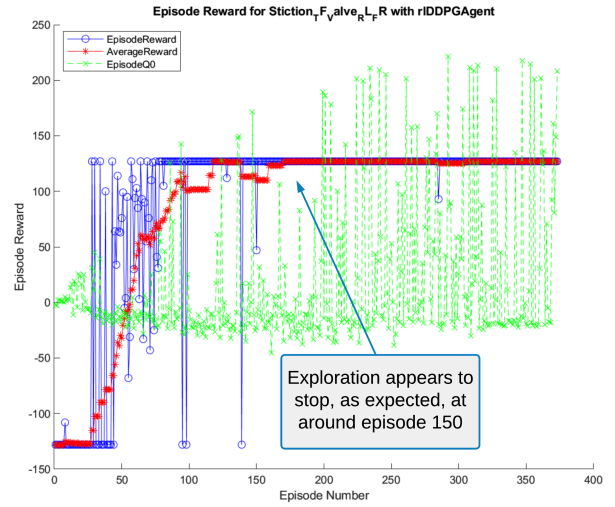
Figure 39: Effect of large reward spaces

6.3.4. Sensitivity to noise parameter

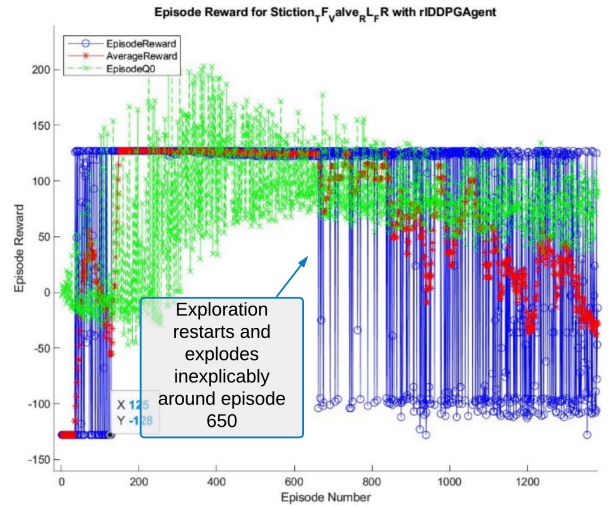
DDPG uses the Ornstein-Uhlenbeck process to aid exploration. The effect of noise hyperparameter was not very easily ascertainable.

Based on (19), for a $VarianceDecayRate = 3 \times 10^{-5}$ and $T_S = 150$ time-steps per full episode, the half-life of exploration decay is about 150 episodes as seen in Fig.40(a). However there is an exploration *explosion* after about 650 episodes (Fig.40(b)). As an experiment a severely reduced $VarianceDecayRate = 3 \times 10^{-4}$ was used implying a half-life of just about 15 episodes, however Fig.41 shows no decay even after 1200 episodes.

It is *possible* that the mixed results agree with (Plappert et al., 2017); explicit noise settings are *not* necessary for a continuous space to assist exploration. It must be noted that such results can also be possible due to inexplicable interaction effects of multiple hyperparameters.



(a) Variance decay-rate= 3×10^{-5} . Exploration decay after 150 episodes



(b) Variance decay-rate= 3×10^{-5} . Exploration explosion after 650 episodes

Figure 40: Effect of OUP parameters on exploration

6.3.5. Sensitivity to random seeds

Intuitively different random seeds should not affect results of a stable process. According to (Henderson et al., 2017), envi-

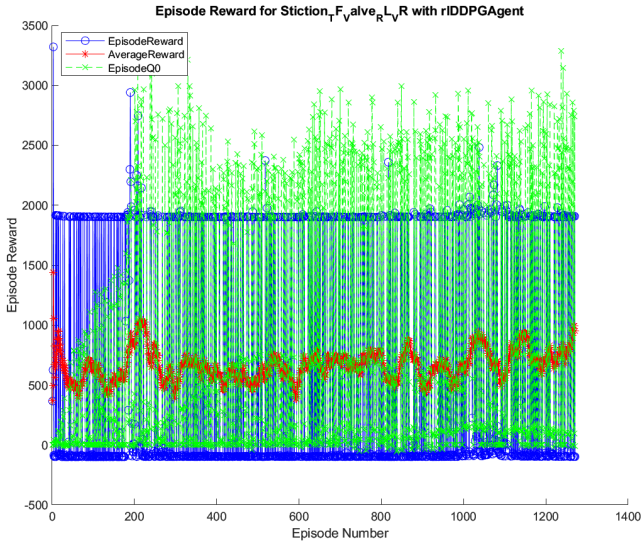


Figure 41: No signs of exploration decay for a decay-rate= 3×10^{-4}

ronment stochasticity coupled with stochasticity in the learning process have produced misleading inferences even when results were scientifically averaged across multiple trials.

In conclusion, as stated by Henderson et al. (2017), one of the possible reasons for the difficulties encountered could be the “intricate interplay” of hyperparameters of policy-gradient methods (such as DDPG).

7. Conclusion

A process of training a model-free reinforcement learning based controller was outlined.

Hyperparameter tuning requires significant efforts and patience, for building a stable controller. We proposed Graded Learning, the naive form of Curriculum Learning, which is shown to avoid several challenges associated with RL training. An engineer starts at the lowest task complexity level, allowing one to easily identify the best hyperparameters, reward strategy and reward scales to apply. The control task complexity is then incremented in steps. For most industrial control systems Table 1 should be a good starting point.

Experiments were conducted to evaluate RL against conventional PID control. RL strategy’s trajectory tracking appears to be superior to the PID’s while the PID demonstrates better disturbance rejection as compared to the disturbances appearing on the RL controlled signal. This appears to be the prime limitation of the RL controller and it must be noted that these were also evident in earlier studies by (Bischoff et al., 2013; Wang et al., 2018) and (Syafie et al., 2008).

The PID appeared to lag the reference control signal while the RL controller performed better when challenged to track a control profile that it was not trained on and will demonstrate versatility when applied to different control tasks within the same environment, without having to be retrained.

Overall the RL controlled process appears to promise better process quality, while the PID controlled process will cause a

significantly lower stress on the valve operation and result in reduced wear-and-tear.

Enhancements and Future work: The RL controller that was designed needs a mechanism to reduce the oscillatory behavior in the presence of high frequency disturbance with strong amplitudes. For noise at the input and output of the controller a low-pass filter may help reduce the high variance.

Further research is necessary to understand ways of defining objective and reward functions to prevent the noisy RL trajectory behaviour. If this succeeds this will be a better solution than applying a filter, which would otherwise slow down the response.

MATLAB 2019b release includes the Proximal Policy Optimization (PPO) algorithm for continuous control that needs evaluation. PPO is a recent development and is considered as being more stable and better than DDPG (Henderson et al., 2017).

The amalgamation of reinforcement learning, optimal-control and control-systems is extremely exciting. It is hoped that this research will motivate further research to help better understand and popularize the use of reinforcement learning for control-systems.

Acknowledgement

This paper is a result of the dissertation submitted to the Coventry University, UK. I am grateful for the guidance of my supervisors Dr. Olivier Haas, Associate Professor and Reader in Applied Control Systems at Coventry University and Dr. Prithvi Sekhar Pagala, Research Specialist at KPIT Technologies. Prof. Dr. Acharya K.N.S must be thanked for instilling an interest in Control Systems through this teaching. The expert comments from reviewers helped improve the quality of this work.

References

- Bischoff, B., Nguyen-Tuong, D., Koller, T., Markert, H., Knoll, A., 2013. Learning throttle valve control using policy search, in: Joint European Conference on Machine Learning and Knowledge Discovery in Databases, Springer. pp. 49–64.
- Bousquet, O., Elisseeff, A., 2002. Stability and generalization. *Journal of machine learning research* 2.
- di Capaci, R.B., Scali, C., 2018. An augmented pid control structure to compensate for valve stiction. *IFAC-PapersOnLine* 51, 799–804.
- Choudhury, M.A.A.S., Shah, S.L., Thornhill, N.F., 2004a. Detection and quantification of control valve stiction. URL: <http://www.sciencedirect.com/science/article/pii/S1474667017319183>.
- Choudhury, M.A.A.S., Thornhill, N.F., Shah, S.L., 2004b. A data-driven model for valve stiction. *IFAC Proceedings Volumes* 37, 245–250.
- Deisenroth, M., Rasmussen, C.E., 2011. Pilco: A model-based and data-efficient approach to policy search, in: Proceedings of the 28th International Conference on machine learning (ICML-11), pp. 465–472.
- Desborough, L., Miller, R., 2002. Increasing customer value of industrial control performance monitoring—honeywell’s experience.
- Duan, Y., Chen, X., Houthoofd, R., Schulman, J., Abbeel, P., 2016. Benchmarking deep reinforcement learning for continuous control.
- Garnier, H., Mensler, M., Richard, A., 2003. Continuous-time model identification from sampled data: implementation issues and performance evaluation. *International Journal of Control* 76, 1337–1357.

- Hardt, M., Recht, B., Singer, Y., 2015. Train faster, generalize better: Stability of stochastic gradient descent.
- He, Q., Wang, J., 2010. Valve stiction modeling: First-principles vs data-drive approaches, in: Proceedings of the 2010 American Control Conference, IEEE. pp. 3777–3782.
- Henderson, P., Islam, R., Bachman, P., Pineau, J., Precup, D., Meger, D., 2017. Deep reinforcement learning that matters .
- Howell, M.N., Best, M.C., 2000. On-line pid tuning for engine idle-speed control using continuous action reinforcement learning automata. Control Engineering Practice 8, 147–154.
- IEEE-GlobalSpec, 1998. Control valves.
- Lewis, F., Vrabie, D., Vamvoudakis, K., 2012. Reinforcement learning and feedback control: Using natural decision methods to design optimal adaptive controllers. URL: <https://ieeexplore.ieee.org/document/6315769>.
- Lillicrap, T.P., Hunt, J.J., Pritzel, A., Heess, N., Erez, T., Tassa, Y., Silver, D., Wierstra, D., 2015. Continuous control with deep reinforcement learning. arXiv preprint arXiv:1509.02971 .
- MathWorks, 2019a. Mathworks announces release 2019a of matlab and simulink. URL: <https://in.mathworks.com/company/newsroom/mathworks-announces-release-2019a-of-matlab-and-simulink.html>.
- MathWorks, 2019b. Matlab: rlddpagentoptions. URL: <https://in.mathworks.com/help/reinforcement-learning/ref/rlddpagentoptions.html>.
- Murray, R., Li, Z., Sastry, S.S., 1994. PID Control. CRC Press. A Mathematical Introduction to Robotic Manipulation, pp. 301–322.
- Narvekar, S., Peng, B., Leonetti, M., Sinapov, J., Taylor, M.E., Stone, P., 2020. Curriculum learning for reinforcement learning domains: A framework and survey. arXiv preprint arXiv:2003.04960 .
- Olivecrona, M., Blaschke, T., Engkvist, O., Chen, H., 2017. Molecular de-novo design through deep reinforcement learning. Journal of Cheminformatics 9.
- openai.com, 2018. Learning dexterity. URL: <https://openai.com/blog/learning-dexterity/>.
- Plappert, M., Houthoofd, R., Dhariwal, P., Sidor, S., Chen, R.Y., Chen, X., Asfour, T., Abbeel, P., Andrychowicz, M., 2017. Parameter space noise for exploration. arXiv preprint arXiv:1706.01905 .
- Popinchalk, S., 2006. Building accurate, realistic simulink models. URL: <https://in.mathworks.com/company/newsletters/articles/building-accurate-realistic-simulink-models.html>.
- Portelas, R., Colas, C., Hofmann, K., Oudeyer, P., 2019. Teacher algorithms for curriculum learning of deep RL in continuously parameterized environments. CoRR abs/1910.07224. URL: <http://arxiv.org/abs/1910.07224>.
- Schoknecht, R., Riedmiller, M., 1999. Using reinforcement learning for engine control. IEE Conference Publication .
- Shoukat Choudhury, M.A.A., Thornhill, N.F., Shah, S.L., 2005. Modelling valve stiction. URL: <http://www.sciencedirect.com/science/article/pii/S09670666104001145>.
- Song, X., Jiang, Y., Tu, S., Du, Y., Neyshabur, B., 2019. Observational overfitting in reinforcement learning URL: <https://arxiv.org/abs/1912.02975>.
- Southampton.ac.uk, . Ground vibration and ground-borne noise from trains. URL: https://www.southampton.ac.uk/engineering/research/groups/dynamics/rail/ground_vibration.page.
- Sutton, R., Barto, A., 2018. Reinforcement Learning: An Introduction. 2nd. edition ed., The MIT Press, Cambridge, England.
- Syafie, S., Vilas, C., Garcia, M.R., Tadeo, F., Alonso, A.A., Martinez, E., 2008. Intelligent control based on reinforcement learning for batch thermal sterilization of canned foods. URL: <http://www.sciencedirect.com/science/article/pii/S1474667016395027>.
- Tedrake, R., 2009. Analytical Optimal Control with the Hamilton-Jacobi-Bellman Sufficiency Theorem. Massachusetts Institute of Technology. Underactuated Robotics: Learning, Planning, and Control for Efficient and Agile Machines Course Notes for MIT 6.832, pp. 74–82.
- Uhlenbeck, G.E., Ornstein, L.S., 1930. On the theory of the brownian motion. Physical review 36, 823.
- Vitelli, M., Nayebi, A., 2016. Carma : A deep reinforcement learning approach to autonomous driving .
- Wang, Y., Velswamy, K., Huang, B., 2018. A novel approach to feedback control with deep reinforcement learning. URL: <http://www.sciencedirect.com/science/article/pii/S2405896318319177>.
- Weiss, K., Khoshgoftaar, T.M., Wang, D., 2016. A survey of transfer learning. Journal of Big data 3, 9.
- Weng, L., 2020. Curriculum for reinforcement learning. lilianweng.github.io/lil-log URL: <https://lilianweng.github.io/lil-log/2020/01/29/curriculum-for-reinforcement-learning.html>.
- Zhang, C., Vinyals, O., Munos, R., Bengio, S., 2018. A study on overfitting in deep reinforcement learning.